Interaction Between Fast and Slow Inactivation in Skm1 Sodium Channels

David E. Featherstone, Janet E. Richmond, and Peter C. Ruben
Department of Biology, Utah State University, Logan, Utah 84322-5305 USA

ABSTRACT Rat skeletal muscle (Skm1) sodium channel α and β_1 subunits were coexpressed in *Xenopus* oocytes, and resulting sodium currents were recorded from on-cell macropatches. First, the kinetics and steady-state probability of both fast and slow inactivation in Skm1 wild type (WT) sodium channels were characterized. Next, we confirmed that mutation of IFM to QQQ (IFM1303QQQ) in the DIII-IV 'inactivation loop' completely removed fast inactivation at all voltages. This mutation was then used to characterize Skm1 slow inactivation without the presence of fast inactivation. The major findings of this paper are as follows: 1) Even with complete removal of fast inactivation by the IFM1303QQQ mutation, slow inactivation remains intact. 2) In WT channels, ~20% of channels fail to slow-inactivate after fast-inactivating, even at very positive potentials. 3) Selective removal of fast inactivation by IFM1303QQQ allows slow inactivation to occur more quickly and completely than in WT. We conclude that fast inactivation reduces the probability of subsequent slow inactivation.

INTRODUCTION

Voltage-gated sodium channels are responsible for the initial rise and subsequent propagation of action potentials in nerve, muscle, and secretory tissues. Therefore, one of the most important determinants of membrane excitability is the availability of sodium channels. The fraction of available sodium channels is governed by two pharmacologically and temporally distinct processes of inactivation: fast inactivation and slow inactivation, both of which have been observed in every sodium channel subtype yet studied, either in native tissue or heterologously expressed channels (Quandt, 1987; Hsu et al., 1993).

The molecular mechanism underlying fast inactivation is now widely accepted to occur as follows: Full or partial activation of the depolarized sodium channel exposes an intracellular binding site for a small number of hydrophobic residues constituting part of the cytoplasmic loop connecting domains III and IV. The subsequent movement and intracellular binding of this fast-inactivation loop blocks conductance (for review, see Catterall, 1993). Fast inactivation is important for action potential termination, spike frequency, and regulation of resting excitability (Hille, 1992).

Slow inactivation may also play an important physiological role by contributing to the regulation of resting sodium channel availability (Ruff et al., 1988) and by aiding in slow activity-dependent changes in excitability such as spike frequency adaptation or burst termination (Sawczuk et al., 1995). Furthermore, at least one mutation known to lead to hyperkalemic periodic paralysis, T698M, disrupts slow inactivation and thus probably contributes to the phenotypic hyperexcitability (Cummins and Sigworth, 1996)

The molecular mechanism underlying slow inactivation, however, is still unknown. Proteolytic removal of fast inactivation by intracellular application of enzymes leaves slow inactivation intact (Valenzuela and Bennett, 1994). Presumably, therefore, no intracellular portion of the channel that is digestible by enzymes is crucial for slow inactivation. Unfortunately, enzymatic treatment raises the possibilities of incomplete removal of fast inactivation and nonselective damage to other channel mechanisms. These issues complicate the interpretation of the observation that intracellular enzymatic removal of fast inactivation alters the kinetics of slow inactivation (Valenzuela and Bennett, 1994). The most complete and selective removal of sodium channel fast inactivation to date was achieved via the mutation of three hydrophobic residues (IFM → QQQ) in the intracellular fast-inactivation loop connecting domains III and IV (West et al., 1992). However, this mutant has not yet been used in a study of sodium channel slow inactivation.

In this paper, we characterize the kinetics and steady-state probability of both fast and slow inactivation in Skm1 wild type (WT) sodium channels. We confirmed that mutation of IFM → QQQ in the III-IV loop (IFM1303QQQ) completely removes fast inactivation at all voltages. Using the IFM1303QQQ mutant, we then characterized slow inactivation in channels lacking fast inactivation. Although fast inactivation was well described by a voltage-dependent, two-state, first-order Eyring reaction model, slow inactivation was only fitted with such a model in the absence of fast inactivation. With fast inactivation present, slow inactivation at positive potentials (−30 mV to +60 mV) occurred more slowly and with less voltage dependence. We hypothesize that fast inactivation induces a partial immobilization of the sodium channel protein, which must be overcome for the channel to enter, but not recover from, the slow-inactivated state. One prediction of this hypothesis is that modulators of fast inactivation may also lead to changes in slow inactivation, even if slow inactivation is not directly affected.

Received for publication 30 May 1996 and in final form 4 September 1996.
Address reprint requests to Dr. David Featherstone, Department of Biology, Utah State University, Logan, UT 84322-5305, Tel.:801-797-2136; Fax: 801-797-1575; E-mail: davef@cc.usu.edu.

0006-3495/96/12/3098/12 $2.00

METHODS

cDNA for Skm1 WT, β subunit, and Skm1 IFM1303QQQ were generously provided by the laboratories of A. Goldin, L. Isom, and J. Patlak, respectively. Full-length 6.4-kb Skm1 sodium channel α-subunit RNA was subcloned from pBluescript into pGH19 plasmid templates and grown in HB101 cells. mRNA was synthesized in vitro with T7 polymerase. β-subunit cDNA in pBluescript was translated in vitro with T3 polymerase. Before in vitro transcription, WT Skm1 sodium channel cDNA was linearized with *Not*I, and β subunit with *Hin*dIII. Expression of the fast-inactivation-removed mutant Skm1, IFM1303QQQ, was improved by subcloning the mutated region into the WT Skm1/pGH19. The IFM mutant mRNA was subsequently linearized with *Not*I and synthesized with T7. For each clone, 1 μg of linearized template was used to perform in vitro transcriptions using mMessage mMachine Kits from Ambion Inc (Austin, TX). RNA for injection was concentrated on polysulfone filter units (Millipore, Bedford, MA) and resuspended in 1 mM Tris-Cl pH 6.5 at a concentration of ~1 μg/μl. Before injection, equal volumes of α- and β-subunit mRNA (each at a concentration of ~1 μg/μl) were mixed together. β subunit in this amount was injected with both WT and IFM1303QQQ α subunits.

Oocytes were surgically removed from female *Xenopus* laevis (Nasco, Modesto, CA) anesthetized with 0.17% tricaine methanesulfonate (Sigma, St. Louis, MO). Theca and follicles were enzymatically removed by gently agitating the oocytes in a solution containing (in mM): NaCl 96, KCl 2, $MgCl_2$ 20, 1,4-(2-hydroxyethyl)-1-piperazineethanesulfonic acid (HEPES) 5, pH 7.4, with 2 mg/ml type IA collagenase (Sigma, St. Louis, MO) for ~1 h. 24 h after enzymatic treatment, oocytes were individually injected with 50 nl of mRNA using a Drummond automatic injector and then placed in sterile incubation media containing (in mM): NaCl 96, KCl 2, $MgCl_2$ 20, $CaCl_2$ 1.8, HEPES 5, Pyruvic acid 2.5, pH 7.4, with 1–5% Horse serum (Irvine Scientific, Irvine, CA) and Gentamycin Sulfate 100 mg/l, where they were incubated with gentle agitation at 18°C until electrophysiological recording 3–14 days later.

Oocytes were prepared for macropatch recording by manually removing the vitelline membrane after short (2–5 min) exposure of the oocytes to a hyperosmotic solution containing (in mM): NaCl 96, KCl 2, $MgCl_2$ 20, HEPES 5, Mannitol 400, pH 7.4. All macropatch recording was done in a bath containing (in mM): NaCl 9.6, KCl 88, EGTA 11, HEPES 5, pH 7.4. Aluminosilicate patch electrodes were pulled in several stages (using a Sutter P-87), dipped in melted dental wax to reduce capacitance, fire polished, and filled with (in mM): NaCl 96, KCl 4, $MgCl_2$ 1, $CaCl_2$ 1.8, HEPES 5, pH 7.4.

Electrophysiological recordings were made using an EPC-9 patch-clamp amplifier (HEKA, Lambrecht, Germany) and digitized at 5 KHz via an ITC-16 interface (Instrutech, Great Neck, NY). Voltage clamping and data acquisition were controlled via Pulse software (HEKA) running on a Power Macintosh 7100/80. All data were software-low-pass-filtered at 5 KHz during acquisition. Experimental bath temperature was maintained at 22 ± 0.2°C for all experiments by using a peltier device controlled by an HCC-100A temperature controller (Dagan, Minneapolis, MN). After seal formation, patches were left on-cell for all recordings. On-cell patches were more stable, allowing long-term recordings, and, because of equal cytosolic and extracellular $[K^+]$, the patches showed no differences in sodium currents or voltage dependence compared to excised inside-out patches. Where the voltage dependence of inactivation was studied, the clamp control software (Pulse) alternated prepulse potentials, such that prepulse potentials were delivered as −160 mV, +10 mV, −155 mV, +5 mV, −150 mV, etc. if the voltage range of −160 mV to +10 mV was to be covered in 5-mV steps. Holding potential was −120 mV to −150 mV. Leak subtraction was performed automatically by the software using a p/4 protocol. The four leak pulses alternated voltage direction from a leak holding potential of −120 mV. Leak pulses were always performed after the test pulse, and sufficient time between protocols was allowed to insure that the leak pulses would have no effect on the data.

Subsequent analysis and graphing were done using Pulsefit (HEKA) and Igor Pro (Wavemetrics, Lake Oswego, OR), both run on a Power Macintosh 7100/80. Simulations were performed on a PC, using Simulation Control Program (SCoP) 3.5 (Simulation Resources, Inc., Berrien Springs, MI), applying microscopic reversibility where appropriate. All statistically derived values, both in the text and in figures, are given as mean ± standard error (SEM). Although only a single fit to averaged data is presented in Figs. 3, 6, and 7, *B-D*, fits were performed for each individual data set to obtain SEM values for the time constants and steady-state availabilities shown in Figs. 4, 7 *A*, and 8. Results obtained using the two methods were not significantly different.

Conductance (voltage) curves were computed using the equation:

$$G = I_{max}/(V_m - E_{rev})$$

where G is conductance, I_{max} represents the peak-test-pulse current, V_m the test-pulse voltage, and E_{rev} the measured reversal potential. Descriptions of test-pulse inactivation rates, given as time constants (τ), were derived from fitting the monoexponential decay of individual currents according to the function:

$$I(t) = \text{Offset} + a_1 \exp(-t/\tau)$$

where $I(t)$ is current amplitude as a function of time, Offset is the plateau amplitude (asymptote), a_1 is the amplitude at time = 0, and τ is the time constant (in ms). Time constants for the onset (and recovery) of inactivation were measured in the same way, except that fits were to peak-current amplitude versus prepulse (or interpulse) duration. Descriptions of first-order, two-state reaction kinetics were derived by fitting τ versus voltage curves according to the following equation:

$$\tau(V_m) = 1/(K_f + K_b)$$

where $\tau(V_m)$ represents the time constant of progression to equilibrium as a function of membrane potential; K_f is the rate of the forward reaction (not inactivated → inactivated), and K_b is the rate of the backward reaction (inactivated → not inactivated). $K_f = A \exp +((z'(1 - d)(V_m - V_0))/kT)$ and $K_b = A \exp -((z'd(V_m - V_0))/kT)$. A = half rate at V_0, z' = total reaction valence (in electronic charge, e); d = fractional barrier distance; V_m = membrane potential (in mV); V_0 = midpoint potential (in mV); k = Boltzmann constant, and T = absolute temperature. K_f and K_b are represented in the text as different Greek letters (α_f, β_f and α_b, β_b), as K_f and K_b cannot be used for more than one reaction. Steady-state probability was then predicted using:

$$p(t\infty) = K_f/(K_f + K_b)$$

where $p(t\infty)$ represents the probability of being inactivated at equilibrium.

RESULTS

Sodium currents were recorded from oocytes 3 or more days after mRNA injection. Two-electrode voltage clamp showed currents with anomolously slow sodium kinetics and low voltage dependence, probably due to slow clamp speed and poor space clamp (Chen and Cannon, 1995). Macropatch sodium current recordings, however, always displayed kinetics and voltage dependence indistinguishable from similar data obtained from native channels in skeletal muscle cells (Numann et al., 1994) or Skm1 (μ1) channels heterologously expressed in mammalian cells (Bendahhou et al., 1995; Wang et al., 1996). α subunits expressed alone showed test-pulse inactivation rates that often followed a two-exponential time course. In our oocytes, as in other studies (Nuss et al., 1995; Yang et al., 1993), coexpression of the β_1 subunit reduced or eliminated the amplitude of the slower of these two exponentials. All of the following results were derived from macropatch recordings using oo

cytes coexpressing both α and β subunits, and only from currents displaying a monoexponential test-pulse decay.

Typical Skm1 WT test-pulse currents to potentials between −80 mV and +60 mV are shown in Fig. 1. Current amplitude peaked at ~−20 mV, and reversal potential was between +40 and +50 mV. Fig. 1, *inset*, shows a mean (± SEM) conductance curve for Skm1 WT (N = 10). A test pulse to 0 mV, which is used in all of the following experiments, opens approximately all of the available channels in both Skm1 WT (Fig. 1, *inset*) and Skm1 QQQ patches (N = 5, conductance curve not shown). As shown in the following figures, the number of "available" channels depended strongly on the potential from which the test pulse stepped (i.e., the prepulse or holding potential). To assure that our $G(V)$ curve measured maximum channel availability, the holding potential for this experiment was −150 mV.

Fast inactivation

Fig. 2 shows typical raw data from Skm1 WT experiments determining the time course of prepulse fast inactivation. In these experiments, the voltage was changed from a holding potential of −150 mV to a prepulse voltage of either −50 mV (e.g., Fig. 2 *A*), −60 mV, −70 mV (e.g., Fig. 2 *B*), −80 mV, −90 mV (e.g., Fig. 2 *C*), −100 mV, −110 mV, or −120 mV. After a specified time (0–300 ms) at the prepulse voltage, the fraction of available current was assayed by a test pulse to 0 mV (see pulse protocol diagrams in Fig. 2). At all prepulse potentials (−50 mV to −120 mV), current amplitude decreased as prepulse duration increased, reflecting fast inactivation of sodium channels. In Fig. 2 *A*, the current produced during a 5-ms prepulse to −50 mV is overlaid as a dark line. Note that the decay of current at −50 mV is identical to the inactivation rate of test pulses after −50-mV prepulses. The simultaneous measurement of prepulse inactivation and test-pulse decay such as this was only possible between −50 and −60 mV, where current was detectable during the prepulse. In every case, however, prepulse inactivation and test-pulse decay in the same patch were identical, confirming that (at least between −50 and −60 mV) prepulse inactivation is due to fast inactivation. Although only 5 ms of data are shown, data were collected for prepulses up to 300-ms long.

Peak-current amplitude was measured for each prepulse duration at eight different voltages and normalized. The results are graphed in Fig. 3 *A*. Single exponentials have been fitted to each of the inactivation curves. (Time constants for the fits in Fig. 3 *A* and 3 *B* are plotted in Fig. 4.) At each voltage, the prepulse fast inactivation was well fitted by a single exponential. Both the prepulse fast-inactivation rate and fraction of fast-inactivated channels increased at more depolarized prepulse potentials. Although not shown for figure clarity, data were collected for prepulse durations up to 300 ms.

Fig. 3 *B* shows Skm1 WT recovery from fast inactivation after 500-ms prepulses to 0 mV. As the time between prepulse and test pulse lengthened, the number of recovered channels increased. Both the rate of recovery and fraction of recovered channels at steady state increased as the interpulse potential (the potential at which recovery was allowed to take place) was made more negative. Fit lines are single exponentials. As in Fig. 2, data were collected for interpulse intervals up to 300 ms in duration, but are not shown for clarity.

In Fig. 4 *A*, Skm1 WT time constants for test-pulse decay, prepulse fast inactivation, and fast recovery are combined in

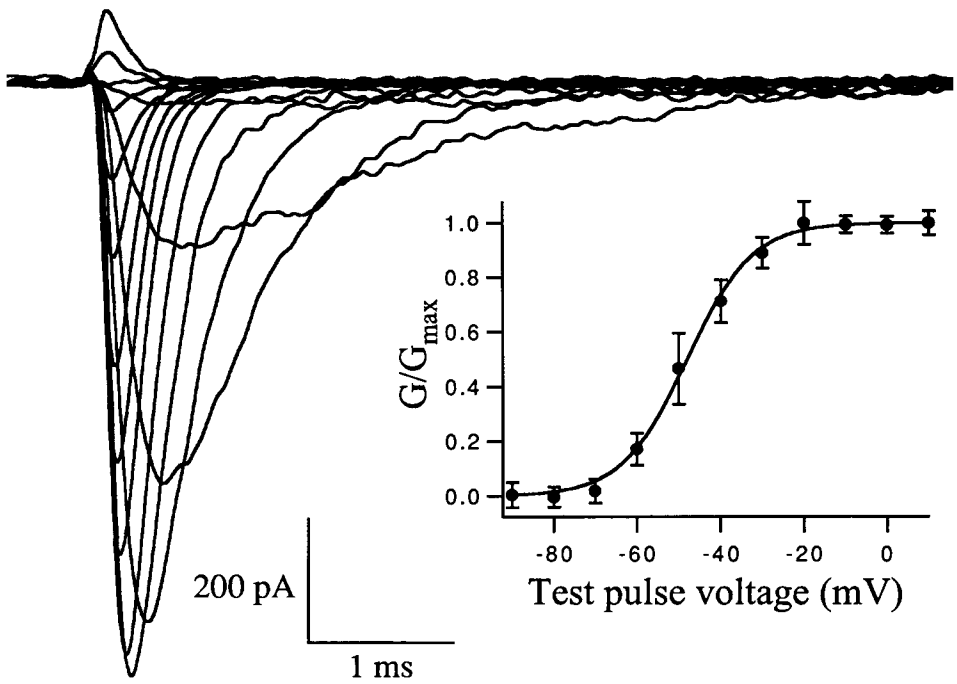

FIGURE 1 Typical sodium currents recorded from macropatches on oocytes expressing rat Skm1 WT sodium channels in response to test pulses from −80 mV to +60 mV in 10-mV increments. *Inset*: A graph of mean (± SEM) Skm1 normalized conductance (G/G_{max}) versus voltage (N = 10).

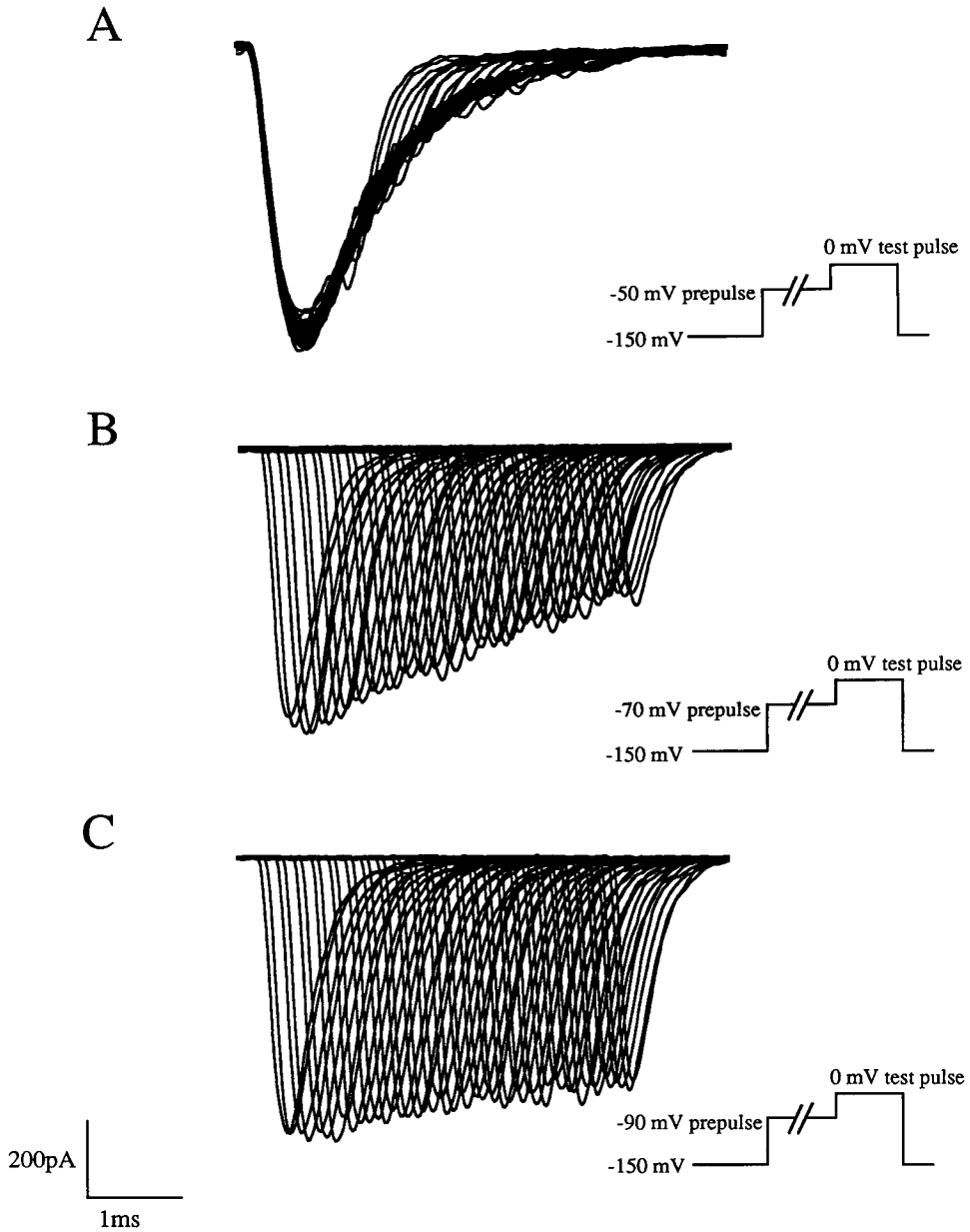

FIGURE 2 Skm1 WT prepulse fast inactivation at three different potentials. In each case, the membrane potential was depolarized from −150 mV to either −50 mV (*A*), −70 mV (*B*), or −90 mV (*C*) for variable lengths of time. Immediately after this prepulse, a pulse to 0 mV assayed for available channels. As the prepulse duration increased, the size of the test-pulse current decreased. When the prepulse was −50 mV (*A*), a substantial current was elicited by the prepulse. This current is darkened for emphasis. Note that the decrease in test-pulse amplitude and prepulse-current decay have the same time course. Although not shown, data were collected to 300 ms.

one graph. Time constants for test-pulse decay were derived from monoexponential fits to decay of test-pulse currents such as those shown in Fig. 1. Time constants for prepulse fast inactivation were derived from monoexponential fits to prepulse fast-inactivation curves such as those shown in Fig. 3 *A*. Time constants for recovery from fast inactivation were derived from monoexponential fits to curves such as those shown in Fig. 3 *B*. Within a single patch, a graph of time constant versus voltage always formed a continuous, bell-shaped curve. From patch to patch, however, variation was observed in the curve's shape. The time constants plotted in Fig. 4 *A* were averaged for each voltage and the averages were fitted by a two-state (not inactivated ↔ inactivated), first-order Eyring reaction model (see Methods). The coefficients of this fit suggest a maximum time constant of 11.3 ms, a total reaction valence of 3.38 *e*, a relative barrier position of 0.51, and a reaction midpoint of −93 mV. Fig. 4 *B* shows that this model (using the same coefficients) also provides a very good prediction (*solid line*) of steady-state fast inactivation, when steady-state values are measured after 500-ms prepulses (*filled squares*). The steady-state values plotted in Fig. 4 *B* are also matched closely by asymptotes of exponential fits to fast-inactivation onset (*open diamonds*) and recovery curves (*open squares*), the averages of which are plotted in Fig. 3.

Fast inactivation was also explored in oocytes expressing a version of Skm1 in which three amino acids (IFM) in the III-IV loop were mutated to glutamines (IFM1303QQQ). Fig. 5 shows the complete absence of prepulse fast inactivation in these mutants at voltages between −120 and −80 mV ($N = 3$). Fig. 5, *inset*, shows example test-pulse currents from the IFM mutant at test potentials between −80

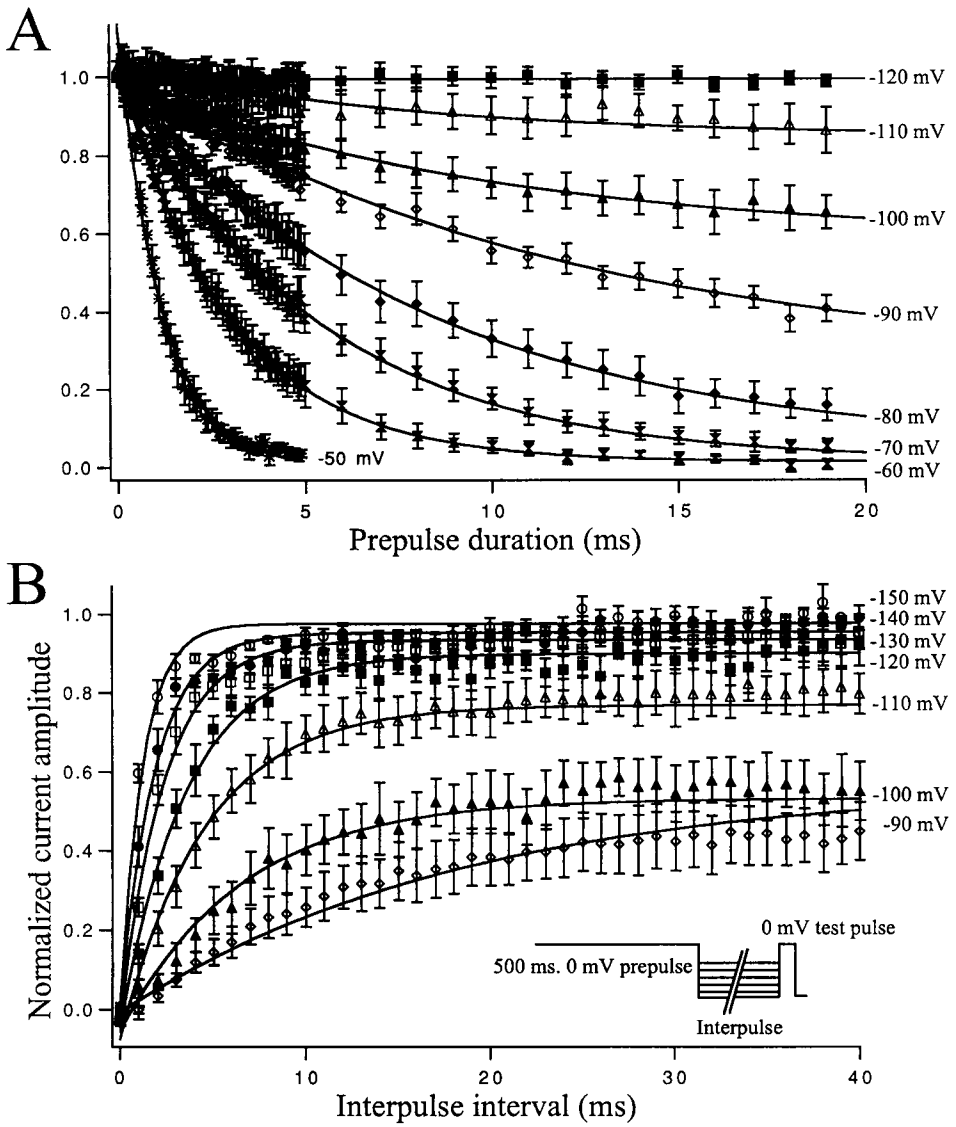

FIGURE 3 Skm1 WT prepulse fast inactivation and recovery over time. For both *A* and *B*, fit lines are single exponentials. Although not shown, data were collected to 300 ms. (*A*) As shown in Fig. 2, the amplitude of currents in response to a 0-mV test pulse decreased as prepulse duration increased. In *A*, normalized test-pulse amplitude is plotted versus prepulse duration, for eight different prepulse potentials: −50 mV (*asterisks*, $N = 4$), −60 mV (*filled hourglasses*, $N = 4$), −70 mV (*open hourglasses*, $N = 4$), −80 mV (*filled diamonds*, $N = 4$), −90 mV (*open diamonds*, $N = 5$), −100 mV (*filled triangles*, $N = 4$), −110 mV (*open triangles*, $N = 4$), and −120 mV (*filled squares*, $N = 4$). Pulse protocols for *A* are as depicted in Fig. 2. (*B*) Channels were fast-inactivated by a 500-ms prepulse to 0 mV, then recovered during interpulses of variable duration and voltage. In *B*, normalized test-pulse-current amplitude (a measure of recovered channels) is plotted versus interpulse duration. data are shown for seven different interpulse voltages: −90 mV (*open diamonds*, $N = 4$), −100 mV (*filled triangles*, $N = 4$), −110 mV (*open triangles*, $N = 4$), −120 mV (*filled squares*, $N = 4$), −130 mV (*open squares*, $N = 4$), −140 mV (*filled circles*, $N = 4$), and −150 mV (*open circles*, $N = 4$).

mV and +60 mV. No test-pulse fast inactivation was apparent at any voltage ($N = 5$). Both open- and closed-state fast inactivation were completely eliminated by the IFM mutation.

Slow inactivation

After very long durations (several seconds to minutes) at depolarized potentials, the Skm1 WT channels entered a slow-inactivated state from which recovery took several seconds, rather than a few milliseconds, as was observed for fast inactivation. To isolate slow inactivation in WT channels, we took advantage of the fact that Skm1 channels recover from fast inactivation within a few milliseconds at very hyperpolarized potentials (see Fig. 4 *A*). Assuming negligible recovery from slow inactivation occurs within 5 ms, fast inactivation's contribution to total prepulse inactivation was eliminated by inserting a 5-ms step to −150 mV between a prepulse and test pulse. Channels fast-inactivated during the prepulse will recover during this 5-ms recovery pulse. Therefore, any inactivation still present in the test pulse, after the recovery pulse, was due solely to slowly

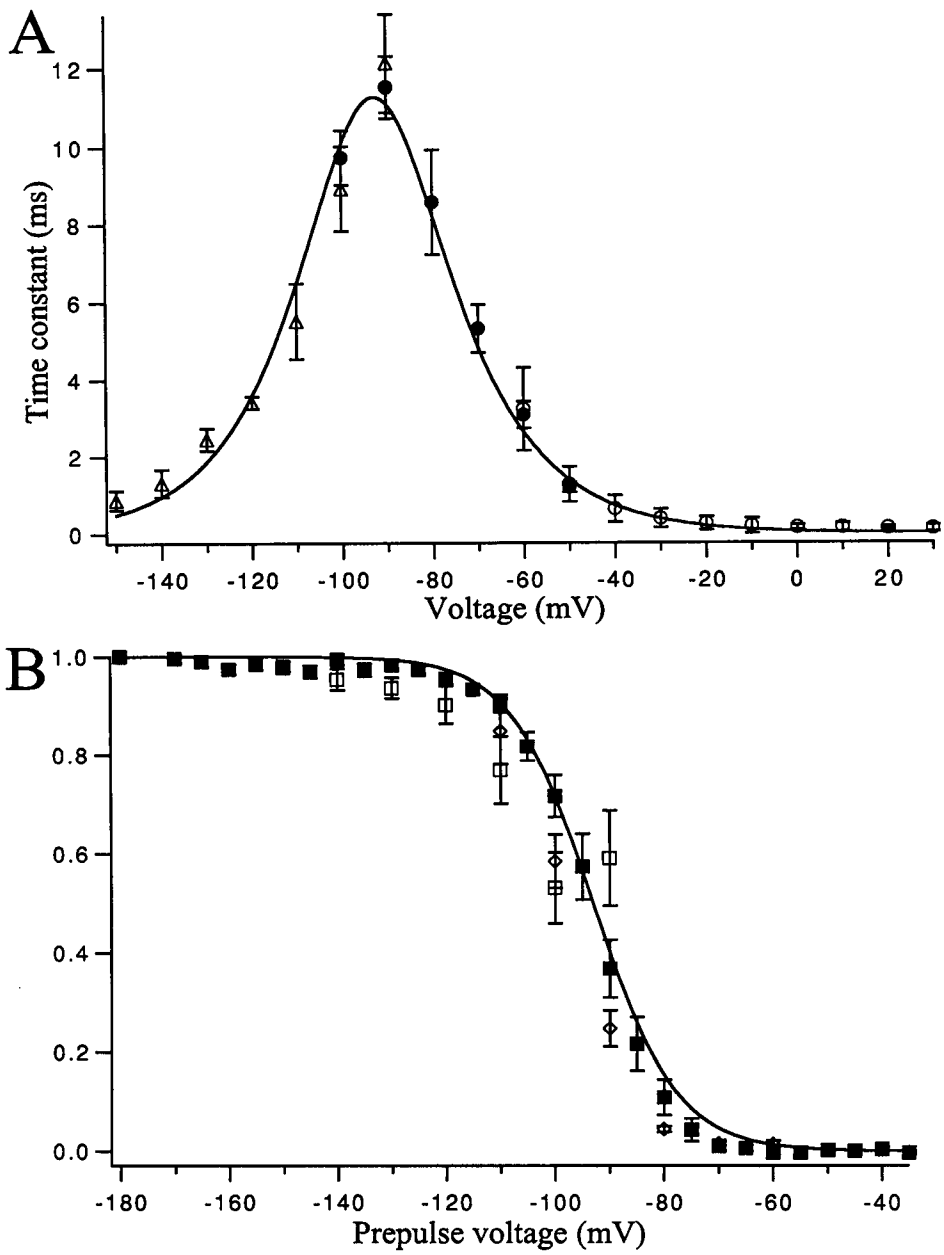

FIGURE 4 (*A*) Skm 1 WT fast-inactivation time constants versus voltage. Time constants were derived from monoexponential fits to fast-inactivation recovery (*open triangles*, $N = 4$), such as shown in Fig. 3 *B*, monoexponential fits to prepulse fast inactivation (*filled circles*, $N = 4$), such as shown in Fig. 3 *A*, or test-pulse decay (*open circles*, $N = 7$), from currents such as those shown in Fig. 1. The fit line is a prediction of a first-order reaction model (see text). (*B*) Skm1 WT steady-state fast inactivation after 500-ms prepulses to various voltages (*filled squares*, $N = 11$), compared to steady-state fast inactivation predicted by asymptotes of monoexponential fits to prepulse fast inactivation (*open diamonds*, $N = 4$), as in Fig. 3 *A*, and recovery (*open squares*, $N = 4$), as in Fig. 3 *B*. The fit line is a prediction of a first-order reaction using the same coefficients as used for the fit in *A*.

recovering slow inactivation. Contamination from any slowly recovering fast-inactivation mode was avoided by analyzing only currents that displayed a monoexponential test-pulse decay. Voltage was clamped to −150 mV for 30 s before every prepulse to insure complete recovery from all inactivation and to avoid any possible accumulation of inactivation throughout the experiment. In steady-state slow-inactivation protocols, voltages were alternated to avoid contaminating the data with time-associated trends.

Fig. 6 *A* shows the time course of Skm1 WT slow inactivation at several prepulse potentials. These data were derived exactly as shown in Fig. 3 *A* except for 1) the much longer prepulse durations (up to 60 s), 2) the addition of the 5-ms, −150-mV fast-inactivation recovery pulse immediately before the test pulse, and 3) 30 s at −150 mV between each data point to allow complete recovery from all inactivation (see protocol diagram in Fig. 6 *A*). Like fast inactivation, the onset rate of slow inactivation and the fraction of slow-inactivated channels both increased at more depolarized potentials, up to −30 mV. Greater than −30 mV, the rate of slow inactivation and the fraction of slow-inactivated channels reached an apparent plateau. (Time constants to individual exponential fits are plotted in Fig. 7 *A*. Asymptotes are plotted in Fig. 8.) Slow-inactivation onset at all potentials was fitted by a single exponential.

Fig. 6 *B* shows the time course of recovery from Skm1 WT slow inactivation at several interpulse potentials. These data were derived exactly as those shown in Fig. 3 *B* except for 1) a prepulse to 0 mV for 60 s was used to slow-inactivate the channels, 2) interpulse durations were much

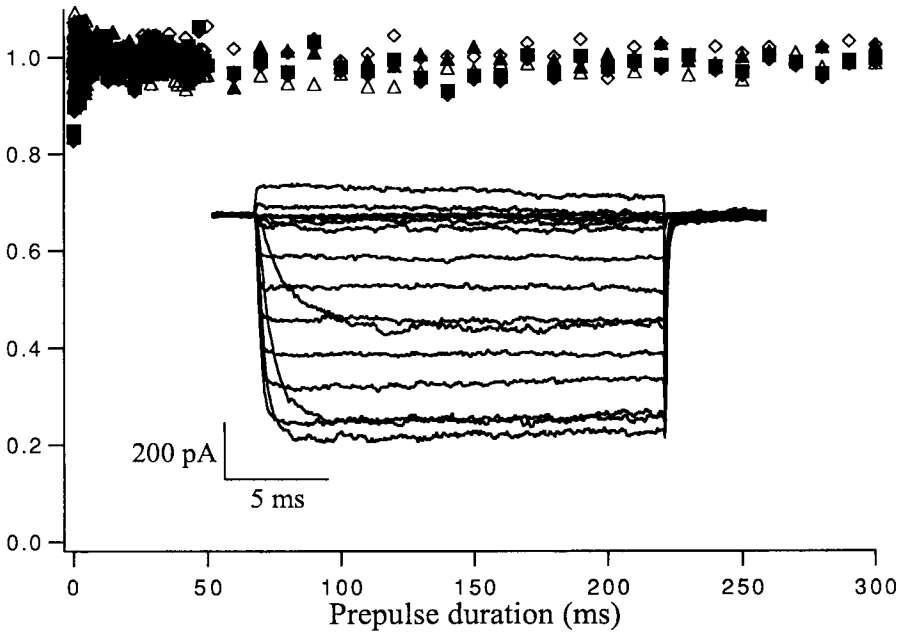

FIGURE 5 Fast inactivation is absent in Skm1 IFM1303QQQ at several different prepulse potentials. Techniques were as described for Figs. 2 and 3 *A*. Typical data (1 of $N = 7$) are shown for prepulses of −80 mV (*filled squares*), −90 mV (*open triangles*), −100 mV (*filled triangles*), −110 mV (*open diamonds*), and −120 mV (*filled diamonds*). *Inset*: An example of (1 of $N = 5$) Skm1 IFM1303QQQ test-pulse currents at test potentials of −90 mV to +60 mV in 10-mV increments.

longer (up to 60 s), 3) a 5-ms, −150-mV recovery pulse was added immediately before the test pulse, and 4) voltage was held at −150 mV for 30 s between each data point to allow complete recovery from all inactivation (see protocol diagram in Fig. 6 *B*). Because not all WT channels slow-inactivated (see Fig. 8), recovery did not always take place from 0 current. Like recovery from fast inactivation, the slow recovery rate and fraction of channels that recovered from slow inactivation increased as the interpulse potential was more hyperpolarized. Recovery from slow inactivation was best fitted by a single exponential (with the exception of the fit to the data recovering from −100 mV where a single exponential loosely approximates the data). Time constants to individual exponential fits are plotted in Fig. 7 *A*. Asymptotes are plotted in Fig. 8 as open circles.

The ability of channels to enter slow inactivation was not eliminated by the IFM mutation. Similar slow-inactivation onset and recovery curves were obtained from the fast-inactivation-removed Skm1 IFM1303QQQ mutant (summarized in Fig. 7 *A*, and shown for selected voltages in Fig. 7, *B-D*).

Fig. 7 *A* shows graphs of time constants versus voltage derived from monoexponential fits to slow-inactivation onset (−90 and above) and recovery (−100 mV and below) curves such as those shown in Figs. 6, *A* and *B*. Each data point was obtained by taking the mean (± SEM) time constant from fits to several (mean $N = 7$) different curves. At potentials more positive than −50 mV, the time constants for Skm1 WT and IFM1303QQQ are significantly ($p < 0.01$) different from each other at each voltage. Unlike the data from IFM1303QQQ, the Skm1 WT curve is asymmetrical: The time constants at the positive (−50 mV and above) end of the curve are significantly ($p < 0.01$) different from those at the negative (−130 mV and below) end of the curve. The IFM1303QQQ mutant data are reasonably well fitted by a first-order, two-state (not inactivated → inactivated) Eyring reaction model (*solid line*) with the following characteristics: maximum time constant of 28.4 s, a total reaction valence of 2.3 *e*, a relative barrier position of 0.55, and a reaction midpoint of −93 mV. The Skm1 WT data, on the other hand, cannot be fitted by a first-order, two-state reaction model (fit attempts not shown), even when no coefficients (including relative barrier distance) are constrained by the fitting program (Igor Pro 3.0) and several starting points are used. A first-order, two-state Eyring reaction equation such as we used (see Methods) cannot simultaneously predict the voltage-dependent time constants at negative voltages and the voltage-independent time constants at positive voltages. The asymmetry is too large.

Fig. 7, *B-D*, shows plots of slow-inactivation recovery at −130 mV (7 *B*), and onset at −30 mV (7 *C*) and 0 mV (7 *D*) for rat Skm WT and IFM1303QQQ. Fit lines are single exponentials. Note the similarity of recovery rates between WT and IFM1303QQQ at −130 mV, but faster slow inactivation of IFM1303QQQ compared to WT at −30 mV and 0 mV.

Mean (± SEM, $N = 7$ WT, $N = 6$ IFM1303QQQ) steady-state (60 s) slow-inactivation curves for both Skm1 WT and IFM1303QQQ are depicted in Fig. 8. Although the fast-inactivation-removed Skm1 mutant appears to slow-inactivate completely within 1 min at potentials more depolarized than ~−50 mV, Skm1 WT often (but not always) fails to slow-inactivate completely, even at potentials as high as +60 mV (not shown on this graph). This difference is significant ($p < .01$) at all potentials more positive than −60 mV. If the apparent failure of WT channels to fully slow-inactivate was due to a failure to reach steady state within 1 min, then asymptotes of exponential fits to the data in Fig. 6 *A* should indicate more inactivation than the WT data shown in Fig. 8. As can be seen in Fig. 8, the asymp

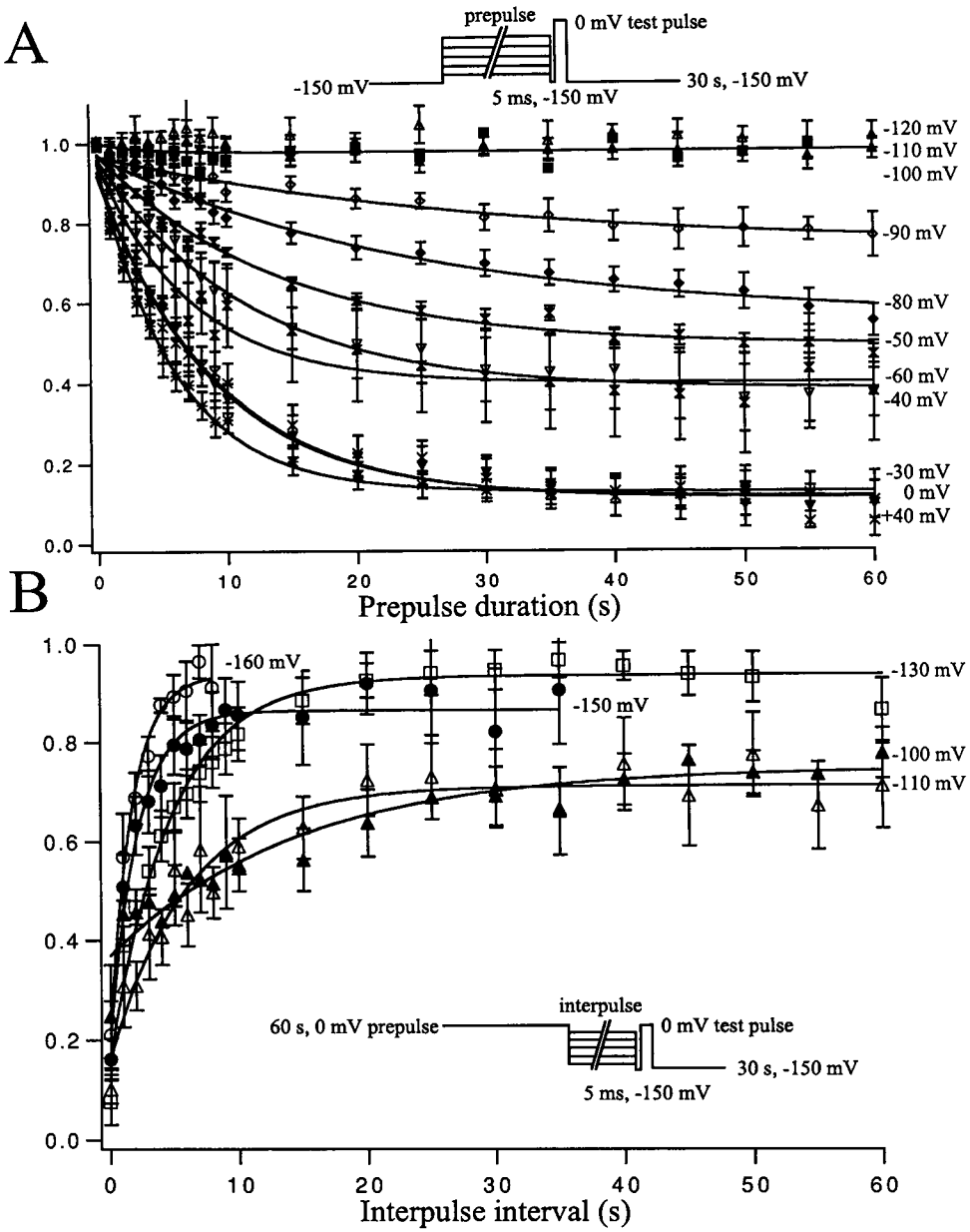

FIGURE 6 Prepulse slow inactivation and recovery in Skm1 WT. (*A*) Membrane potential was changed from −150 mV to a prepulse potential of either +40 mV (*crosses*, $N = 11$), 0 mV (*asterisks*, $N = 17$), −30 mV (*filled upside-down triangles*, $N = 6$), −40 mV (*open upside-down triangles*, $N = 3$), −50 mV (*filled hourglasses*, $N = 5$), −60 mV (*open hourglasses*, $N = 5$), −80 mV (*filled diamonds*, $N = 6$), −90 mV (*open diamonds*, $N = 4$), −100 mV (*filled triangles*, $N = 4$), −110 mV (*open triangles*, $N = 12$), and −120 mV (*filled squares*, $N = 4$). Immediately after the prepulse, a pulse to −150 mV for 5 ms selectively removed fast inactivation. A test pulse to 0 mV then assayed for available channels. 30 s at −150 mV was allowed between each measurement to recover from slow inactivation. As the prepulse duration increased, the size of the test-pulse current decreased. Fit lines are single exponentials. (*B*) Channels were inactivated by a 60-s prepulse to 0 mV, then recovered during interpulses of variable duration and voltage. A step to −150 mV for 5 ms selectively recovered fast-inactivated channels immediately before the test pulse. 30 s at −150 mV was allowed between each measurement to avoid accumulation of slow inactivation. Normalized test-pulse-current amplitude is plotted versus interpulse duration. Data are shown for five different interpulse voltages: −100 mV (*open triangles*, $N = 4$), −110 mV (*closed triangles*, $N = 12$), −130 mV (*open squares*, $N = 5$), −150 mV (*filled circles*, $N = 4$), and −160 mV (*open circles*, $N = 4$). Fit lines are single exponentials. Because current did not always completely slow-inactivate, recovery in most cases did not begin from a normalized current amplitude of 0.

totes (superimposed in Fig. 8 as *open circles*) are similar to the data after a 1-min prepulse, suggesting steady state was attained during a 60-s prepulse. Individual asymptotic fits to slow recovery (*open squares*) also approximate the steady-state curve.

Both fast and slow inactivation occur in Skm1 WT sodium channels. Our data suggest that maximal fast inactivation is reached within a few tens of milliseconds. If the membrane is depolarized longer, does slow inactivation contribute to total steady-state inactivation, thus further

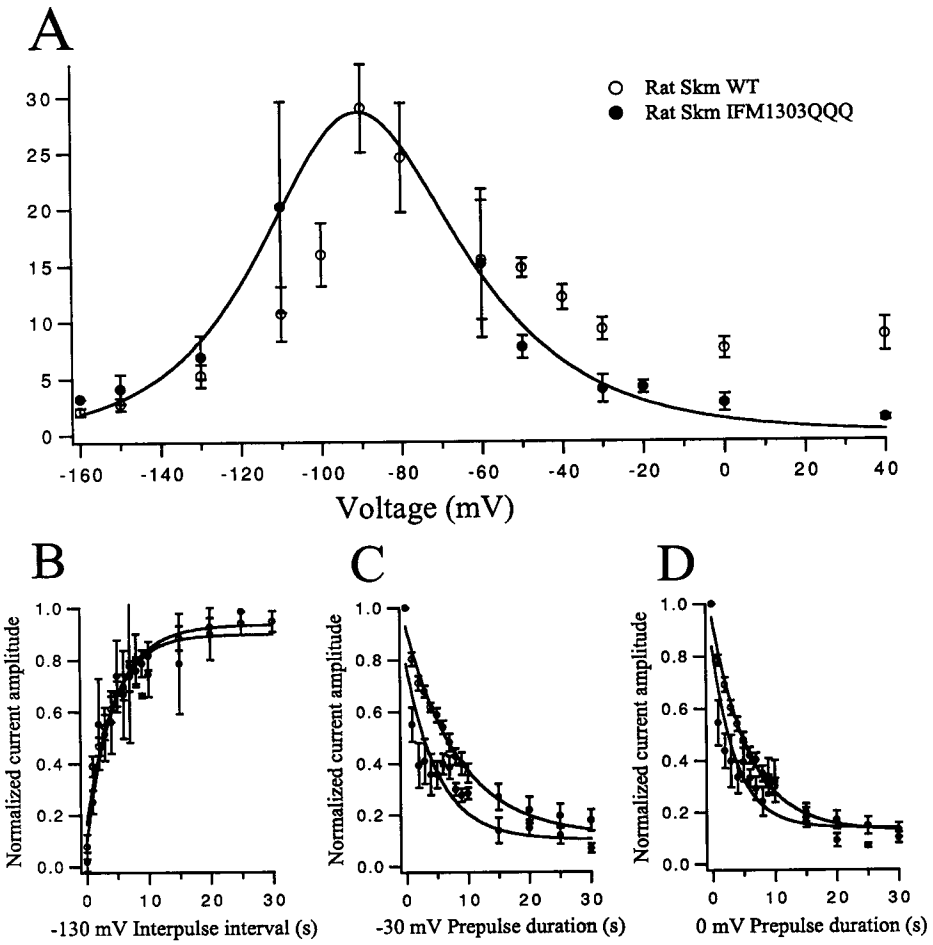

FIGURE 7 (*A*) Time constants of slow inactivation versus voltage, for Skm1 WT (*open circles*) and IFM1303QQQ (*filled circles*). Time constants were derived from monoexponential fits to individual onset (−90 mV and above) or recovery (−100 mV and below) curves of slow inactivation such as shown in Fig. 6. The fit line is a prediction of a first-order reaction model (see text) to IFM1303QQQ. (*B-D*) Examples of averaged slow-inactivation recovery (*B*) and onset curves (*C* and *D*) for Skm1 WT (*open circles*) and IFM1303QQQ (*filled circles*).

reducing the immediate availability of channels at any potential? In Fig. 9, steady-state fast inactivation (*open circles*) and steady-state slow inactivation (*open squares*) are plotted with total steady-state inactivation (*closed circles*) produced by a 1-min prepulse without a 5-ms prepulse to recover fast inactivation (see diagram in Fig. 9). Total steady-state inactivation is not significantly different from steady-state fast inactivation. Therefore, steady-state inac

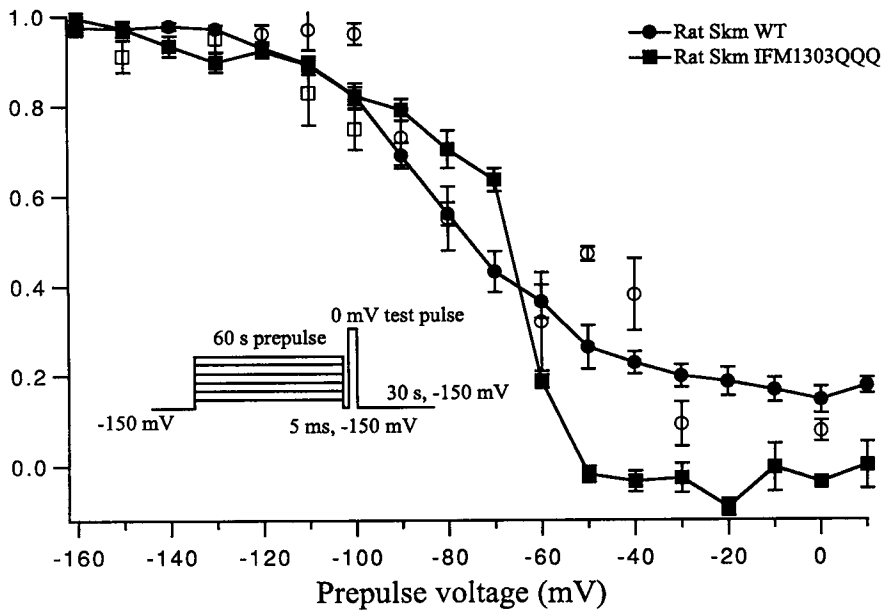

FIGURE 8 Steady-state slow inactivation in Skm1 WT (*filled circles*, $N = 7$) and IFM1303QQQ (*filled squares*, $N = 6$) after a 60-s prepulse to various voltages. Also shown are steady-state values predicted from asymptotes of monoexponential fits to onset (*open circles*) and recovery (*open squares*) from slow inactivation, as shown in Fig. 6. A step to −150 mV for 5 ms was used to selectively recover fast inactivation immediately before the test pulse. 30 s at −150 mV was allowed between each measurement to avoid accumulation of slow inactivation, and voltage steps were alternated: −160 mV, +10 mV, −150 mV, 0 mV, −140 mV, −10 mV, etc. to avoid time- or pulsing-related artifacts.

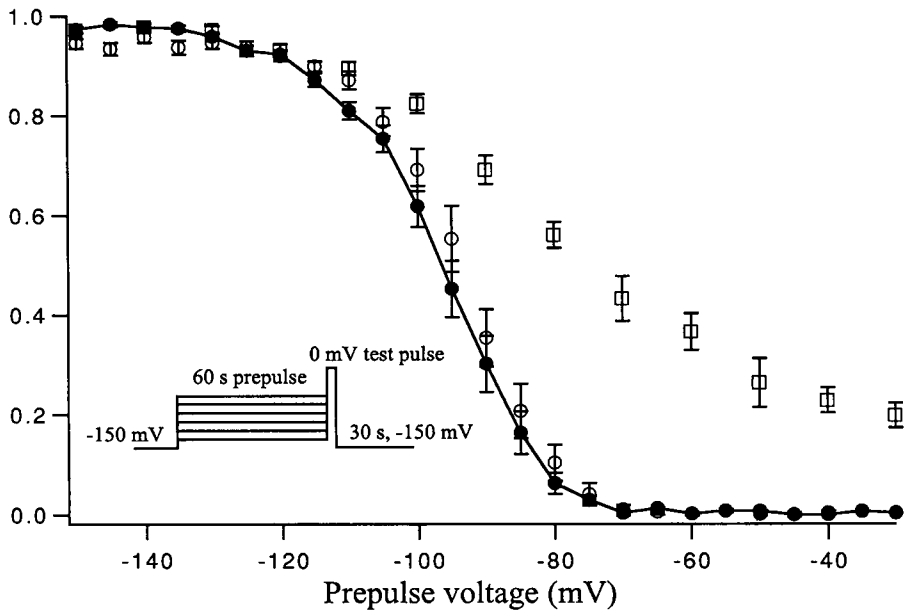

FIGURE 9 Total steady-state inactivation (*filled circles*, $N = 6$) measured immediately after a 60-s prepulse (no hyperpolarizing pulse to recover fast inactivation was used before the test pulse). Open circles show steady-state fast inactivation ($N = 11$) and open squares show steady-state slow inactivation ($N = 7$).

tivation was reached within 500 ms. Longer prepulses produced no further net inactivation. As prepulse duration increased, however, the ratio of slow-inactivated:fast-inactivated channels (which both contribute to total inactivation) gradually increased, eventually producing a steady-state distribution between noninactivated, fast-inactivated, and slow-inactivated channels.

DISCUSSION

The goals of this paper are 1) to provide a basic kinetic characterization of Skm1 sodium channel inactivation on which we can base future studies investigating the mechanisms and modulation of slow inactivation, and 2) to clarify the relationship between fast inactivation and the kinetics of slow inactivation by using selective removal of fast inactivation by site-directed mutagenesis (Skm1 IFM1303QQQ).

Our WT data show that heterologously expressed rat skeletal muscle (Skm1) sodium channels undergo both fast and slow inactivation. Our slow-inactivation measurements from heterologously expressed Skm1 channels are very similar to slow-inactivation measurements made from native sodium channel populations in rat muscle fibers (Ruff et al., 1988). In particular, our measurements of the voltage dependence of Skm1 slow inactivation most closely match slow-inactivation values for fast-twitch (Extensor digitorum longus) muscle, rather than slow-twitch (soleus) muscle (Ruff et al., 1988; Ruff and Whittlesey, 1993a). Skm1 was cloned from rat fast-twitch (Extensor digitorum longus) muscle (Trimmer et al., 1989).

Although published studies of rat skeletal muscle did not use potentials positive enough to determine whether a fraction of non-slow-inactivating channels exist, native cardiac muscle sodium channels (Valenzuela and Bennett, 1994) show the same failure to fully slow-inactivate at positive potentials as the heterologously expressed Skm1 WT channels in this study.

Skm1 fast and slow inactivation were similar in that the fraction of inactivated channels and the rate of inactivation both increased at more positive potentials. Slow inactivation, however, was over 3 orders of magnitude slower than fast inactivation. In Skm1 WT, but not Skm1 IFM1303QQQ, slow-inactivation rates reached an apparent plateau at potentials more positive than ~ -30 mV, and on average almost one-fifth of the channels failed to slow-inactivate at all. When fast inactivation was absent (in IFM1303QQQ), channels fully slow-inactivated at positive potentials. Our data are consistent with other studies of sodium channel slow inactivation, in which slow-inactivation rates increased after enzymatic removal of fast inactivation (Rudy, 1978; Valenzuela and Bennett, 1994). Thus, the acceleration of slow inactivation observed after enzymatic removal of fast inactivation is probably not an artifact of nonselective digestion.

Although our slow-inactivation measurements were similar to those made in native channels, the voltage dependence of fast inactivation measured in our study was left-shifted compared to some accounts of fast inactivation in native rat muscle channels. In studies of native channels, the voltage that fast-inactivates 50% of channels is most often ~ -75 mV (Ruff et al., 1988). This value would predict very little fast inactivation at a muscle resting potential of ~ -90 mV (Ganong, 1995), where approximately one-third to one-half of sodium channels would be slow-inactivated. Unfortunately, $V_{0.5}$ measurements for fast inactivation in native skeletal muscle sodium channels vary between -70 mV and -101 mV, depending on the method used (Ruff et al., 1987). Our $V_{0.5}$ for fast inactivation of -93 mV is within this range. Our measurements of the voltage dependence of fast, slow, and fast + slow inactivation of Skm1 in

oocytes (see Fig. 9) predict that at a resting potential of −90 mV, sodium channels would be distributed approximately equally between fast-inactivated, slow-inactivated, and noninactivated (one-third of the channels in each state).

Modeling sodium channel fast and slow inactivation

In Fig. 4, we show that the kinetics of fast inactivation can be accurately reproduced by a voltage-dependent, first-order, two-state Eyring reaction. Similarly, Fig. 7 *A* suggests that slow inactivation (once fast inactivation has been removed) can also be modeled by a simple two-state reaction. Presumably, therefore, a kinetic model of the sodium channel that accounts for both fast and slow inactivation would include two first-order reactions: one for fast inactivation and one for slow inactivation. We have determined the characteristics of each reaction directly from the fits shown in Figs. 4 and 7 *A*. The rate constants for the fast-inactivation reaction are: $\alpha_f = 0.0444 \exp +((3.3e * (1 - 0.51)(V_m - (-93\ mV)))/25)$, and $\alpha_b = 0.0444 \exp -((3.3e * 0.51(V_m - (-93\ mV)))/25)$ for the onset and recovery of fast inactivation, respectively. The rate constants for slow inactivation are: $\beta_f = 0.0000176 \exp +((2.3e * (1 - 0.55)(V_m - (-93\ mV)))/25)$ and $\beta_b = 0.0000176 \exp -((2.23e * 0.56(V_m - (-93\ mV)))/25)$ for the onset and recovery of slow inactivation, respectively. The simplest model containing these two first-order reactions is as follows:

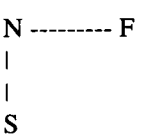

Where the N (noninactivated) ↔ F (fast-inactivated) reaction would be defined by α_f and α_b, and the N ↔ S (slow-inactivated) reaction would be defined by β_f and β_b. Although this type of model does not differentiate between closed or open states, it is a valid approximation of channel inactivation as long as inactivation rates are slow enough compared to other transitions (between closed-closed or closed-open states) so that the eigenvalues for inactivation overwhelmingly dominate. This model allows for slow inactivation in the absence of fast inactivation, and even predicts that slow inactivation will be faster in the absence of fast inactivation. Entry and exit from slow inactivation in this model was simulated in an effort to reproduce data such as shown in Fig. 6. The simulation results were fitted with exponentials and analyzed using the same methods used for our Skm1 data. Unfortunately, simulations using the three-state model pictured above failed to fit either the $\tau(V_m)$ curve for slow inactivation shown in Fig. 7 or the steady-state proportions of slow inactivation in Fig. 8.

The three-state model pictured above, however, does not include a transition between the fast- and slow-inactivated states. Rudy (1978), Valenzuela and Bennett (1994), and Ruff (1996) argue that such a transition exists. A first-order transition could simply be placed between states F and N. If this transition is slow (approximately equal to the rate between N and S, β), the three-state, three-reaction model approximates the rSkm1 IFM1303QQQ slow-inactivation $\tau(V_m)$ curve. The slow-inactivation $\tau(V_m)$ plateau at positive potentials and failure of all channels at positive potentials to slow-inactivate could conceivably be duplicated by manipulating the F ↔ S transition, but the model would still imply that fast and slow inactivation are mutually exclusive states (fast and slow inactivation cannot exist at the same time).

There is reason to believe that fast and slow inactivation are not mutually exclusive states. Enzymatic removal of fast inactivation occurs at a slower rate when channels are depolarized, probably because the III-IV fast-inactivation loop, when bound, is less accessible to proteolytic degradation (Salgado et al., 1985). Degradation rates, however, were also slowed under conditions in which sodium channels would be maximally slow-inactivated (−30 mV for several minutes), implying that the fast-inactivation loop remains bound under slow-inactivated conditions. Also, fast immobilization (and recovery) of gating charge due to fast inactivation occurs when channels are slow-inactivated (Bezanilla et al., 1982), a result inconsistent with models of sequential, mutually exclusive fast- and slow-inactivated states.

A model in which fast and slow inactivation are not mutually exclusive states can be represented by the addition of a fourth state: fast + slow-inactivated.

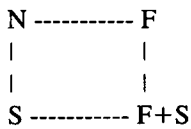

With either one of the models described above, however, difficulty arises in trying to duplicate the fact that steady-state slow inactivation is right shifted relative to the slow-inactivation $\tau(V_m)$ curve in both our data and in native sodium channels. Our slow-inactivation measurements in oocytes show that the time constants of slow inactivation (Fig. 7 *A*) suggest a reaction midpoint of ~−90 mV, but the steady-state slow-inactivation curves (for both mutant and WT) are right shifted, with midpoints of ~−70 mV (Fig. 8). This right shift of steady-state slow inactivation relative to the maximum slow-inactivation time constant τ is also displayed by native skeletal muscle channels (Rudy, 1978; Ruff et al., 1987; Simoncini and Stuhmer, 1987; Ruff et al., 1988; Ruff and Whittlesey, 1993b).

It is conceivable that this difference in slow-inactivation $\tau(V_m)$ midpoint and steady-state slow inactivation is a result of the interaction between slow and fast inactivation. In other words, channels that would otherwise be slow-inactivated might be partially trapped by fast inactivation (which would lead to fewer slow-inactivated channels and a right-shifted steady-state slow-inactivation curve). However, the difference in midpoint of steady-state slow inactivation and the $\tau(V_m)$ of slow inactivation also appears in the

IFM1303QQQ data. If the right shift of steady-state slow inactivation is due to an interaction, then we must conclude that the IFM → QQQ mutation still allows a fast-inactivated state. In fact, it is quite plausible that IFM → QQQ merely leads to loss of channel blockage, even though the channel is otherwise fast-inactivated (i.e., the binding site for the inactivation loop exists). Ultimately, we feel that before an accurate kinetic model of slow inactivation can be created, several issues need to be resolved experimentally (e.g., are fast and slow inactivation mutually exclusive states? Is the channel still fast-inactivated without conductance block in IFM1303QQQ?).

It is tempting, however, to speculate on the reason slow inactivation occurs faster and with more likelihood in the absence of fast inactivation. Fast inactivation has been shown to immobilize gating charge (Armstrong and Bezanilla, 1977). Gating currents are produced by the movement of one or more of the four α-helical S4 transmembrane segments (Yang et al., 1996). Fast-gating charge immobilization therefore implies partial or complete immobilization of one or more S4 segments. If slow inactivation depends on mobility of the S4 segments, or S4 immobilization is concurrent with immobilization of the slow-inactivation mechanism, then fast inactivation with its resulting immobilization of gating charge could plausibly result in channels slow-inactivating more slowly and less completely, as is shown by our data.

The authors would like to thank Esther Fujimoto for the molecular biology, Martin Rayner for reaction modeling advice and critical reading of the manuscript, Clay Prince for TEV, the lab of J. Patlak, for mutant (IFM1303QQQ) Skm1 cDNA, the lab of A. Goldin for Skm1 α-subunit cDNA, and the lab of L. Isom for β-subunit cDNA. This work was supported by PHS grant R-01 NS29204 to PCR.

REFERENCES

Armstrong, C. M., and F. Bezanilla. 1977. Inactivation of the sodium channel. II. Gating current experiments. *J. Gen. Physiol.* 70:567–590.

Bendahhou, S., T. R. Cummins, J. F. Potts, J. Tong, and W. S. Agnew. 1995. Serine-1321-independent regulation of the μ1 adult skeletal muscle Na^+ channel by protein kinase C. *Proc. Natl. Acad. Sci. USA.* 92:12003–12007.

Bezanilla, F., R. E. Taylor, and J. Fernandez. 1982. Distribution and kinetics of membrane dielectric polarization. *J. Gen. Physiol.* 79:21–40.

Catterall, W. A. 1993. Structure and function of voltage-gated ion channels. *Trends Neurosci.* 16:500–506.

Chen, C., and S. C. Cannon. 1995. Modulation of Na^+ channel inactivation by the β_1 subunit: a deletion analysis. *Pflügers Arch.* 431:186–195.

Cummins, T. R., and F. J. Sigworth. 1996. Impaired slow inactivation in mutant sodium channels. *Biophys. J.* 71:227–236.

Ganong, W. F. 1995. Review of Medical Physiology. Appleton & Lange, Norwalk, CT.

Hille, B. 1992. Ionic Channels of Excitable Membranes. Sinauer Associates, Sunderland, UK.

Hsu, H., E. Huang, X.-C. Yang, A. Karschin, C. Labarca, A. Figl, B. Ho, N. Davidson, and H. A. Lester. 1993. Slow and incomplete inactivations of voltage-gated channels dominate encoding in synthetic neurons. *Biophys. J.* 65:1196–1206.

Numann, R., S. D. Hauschka, W. A. Catterall, and T. Scheuer. 1994. Modulation of skeletal muscle sodium channels in a satellite cell line by protein kinase C. *J. Neurosci.* 14:4226–4236.

Nuss, H. B., N. Chiamvimonvat, M. T. Perez-Garcia, G. F. Tomaselli, and E. Marban. 1995. Functional association of the β_1 subunit with human cardiac (hH1) and rat skeletal muscle (μ1) sodium channel α subunits expressed in *Xenopus* oocytes. *J. Gen. Physiol.* 106:1171–1191.

Quandt, F. N. 1987. Burst kinetics of sodium channels which lack fast inactivation in mouse neuroblastoma cells. *J. Physiol.* 392:563–585.

Rudy, B. 1978. Slow inactivation of the sodium conductance in squid giant axons. Pronase resistance. *J. Physiol.* 283:1–21.

Rudy, B. 1981. Inactivation in *Myxicola* giant axons responsible for slow and accumulative adaptation phenomena. *J. Physiol.* 312:531–549.

Ruff, R. L. 1996. Single channel study of slow inactivation of Na^+ channels. *Biophys. J.* 70:A132.

Ruff, R. L., L. Simoncini, and W. Stuhmer. 1987. Comparison between slow sodium channel inactivation in rat slow- and fast-twitch muscle. *J. Physiol.* 383:339–348.

Ruff, R. L., L. Simoncini, and W. Stuhmer. 1988. Slow sodium channel inactivation in mammalian muscle: a possible role in regulating excitability. *Muscle & Nerve.* 11:502–510.

Ruff, R. L., and D. Whittlesey. 1993a. Comparison of Na^+ currents from type IIa and IIb human intercostal muscle fibers. *Am. J. Physiol.* 265: C171–C177.

Ruff, R. L., and D. Whittlesey. 1993b. Na^+ currents near and away from endplates on human fast and slow twitch muscle fibers. *Muscle & Nerve.* 16:922–929.

Salgado, V. L., J. Z. Yeh, and T. Narahashi. 1985. Voltage-dependent removal of sodium inactivation by *N*-bromoacetamide and pronase. *Biophys. J.* 47:567–571.

Simoncini, L., and W. Stuhmer. 1987. Slow sodium channel inactivation in rat fast-twitch muscle. *J. Physiol.* 383:327–337.

Sawczuk, A., R. K. Powers, and M. D. Binder. 1995. Spike frequency adaptation studied in hypoglossal motoneurons of the rat. *J. Neurophysiol.* 73:1799–1810.

Trimmer, J. S., S. S. Cooperman, S. A. Tomiko, J. Zhou, S. M. Crean, M. B. Boyle, R. G. Kallen, Z. Sheng, R. L. Barchi, F. J. Sigworth, R. H. Goodman, W. S. Agnew, and G. Mandel. 1989. Primary structure and functional expression of a mammalian skeletal muscle sodium channel. *Neuron.* 3:33–49.

Valenzuela, C. P., and B. Bennett. 1994. Gating of cardiac Na^+ channels in excised membrane patches after modification by α-chymotrypsin. *Biophys. J.* 67:161–171.

Wang, D. W., A. L. George, Jr., and P. B. Bennett. 1996. Comparison of heterologously expressed human cardiac and skeletal muscle sodium channels. *Biophys. J.* 70:238–245.

West, J. W., D. E. Patton, T. Scheuer, Y. Wang, A. L. Goldin, and W. A. Catterall. 1992. A cluster of hydrophobic amino acid residues required for fast Na^+-channel inactivation. *Proc. Natl. Acad. Sci. USA.* 89: 10910–10914.

Yang, J. S., P. B. Bennett, N. Makita, A. L. George, and R. L. Barchi. 1993. Expression of the sodium channel β_1 subunit in rat skeletal muscle is selectively associated with the tetrodotoxin-sensitive α subunit isoform. *Neuron.* 11:915–922.

Yang, N., A. L. George, Jr., and R. Horn. 1996. Molecular basis of charge movement in voltage-gated sodium channels. *Neuron.* 16:113–122.